Montclair State University
Montclair State University Digital Commons

Department of Earth and Environmental Studies
Faculty Scholarship and Creative Works

Department of Earth and Environmental Studies

Orbitally Paced Shifts in the Particle Size of Antarctic Continental Shelf Sediments in Response to Ice Dynamics during the Miocene Climatic Optimum

Sandra Passchier
Montclair State University, passchiers@montclair.edu

Candice J. Falk

Fabio Florindo
Istituto Nazionale di Geofisica e Vulcanologia

Follow this and additional works at: https://digitalcommons.montclair.edu/earth-environ-studies-facpubs

Part of the Geology Commons, and the Sedimentology Commons

Orbitally paced shifts in the particle size of Antarctic continental shelf sediments in response to ice dynamics during the Miocene climatic optimum

S. Passchier[1], C.J. Falk[1], and F. Florindo[2]

[1]*Department of Earth and Environmental Studies, Montclair State University, 252 Mallory Hall, 1 Normal Avenue, Montclair, New Jersey 07043, USA*

[2]*Istituto Nazionale di Geofisica e Vulcanologia, Via di Vigna Murata, 605, 00143 Rome, Italy*

ABSTRACT

The AND-2A drill hole (ANDRILL [Antarctic Geological Drilling Program] Southern McMurdo Sound Project), ~10 km from the East Antarctica coastline, records nearly 6 m.y. of sedimentation across the Miocene climatic optimum at a high-latitude site. Sedimentological studies of bedforms and particle size distributions indicate that the paleoenvironment was strongly affected by waves and currents, consistent with deposition in a glacially influenced neritic environment. We document abrupt shifts in mud percent within glacial-interglacial cycles ca. 17.8 Ma and between ca. 16.7 and 15.7 Ma that we attribute to the hydrodynamic effects of wave stirring tied to episodes of ice growth and decay. Although wave climate and geodynamic forcing of the paleobathymetry simultaneously affect wave stirring on a high-latitude shelf, both are ultimately controlled by the size of the ice sheet. The mud percent record displays cyclicity at short-eccentricity time scales (94–99 k.y.) and, unexpectedly, ice retreat phases interpreted from the particle size record coincide with eccentricity minima. We attribute the eccentricity-paced ice retreat phases during the late Early Miocene polythermal glacial conditions and the cool orbital parameters to marine ice sheet instability in response to changes in ocean circulation and heat transport. The particle size record of the AND-2A core provides unique near-field evidence for orbitally paced changes in high-latitude climate and ice volume during the Miocene climatic optimum and important insights into the mechanisms of ice sheet growth and decay in a period of global warmth.

INTRODUCTION

Knowing how large ice masses and associated sea ice respond to external forcing is of vital importance because of their role in the Earth's heat balance and global sea-level variations. The Miocene climatic optimum (ca. 17–14.7 Ma) is characterized by extensive faunal and floral turnovers, global sea-level changes, high concentrations of atmospheric CO_2, and the most depleted benthic $\delta^{18}O_{seawater}$ in the past 27 m.y. (Flower and Kennett, 1994; Billups and Shrag, 2002; John et al., 2011; Foster et al., 2012). During this time, the Antarctic ice sheet retreated from the continental shelf into the upland regions of the Transantarctic Mountains (Lewis et al., 2007; Passchier et al., 2011; Hauptvogel and Passchier, 2012).

Although it is known that the Antarctic ice sheet generally responded to orbital cyclicity with an oscillating margin in the marine environment (Naish et al., 2001), ice dynamics during warm periods have previously been poorly constrained. Due to the poor preservation of carbonate in sediments from high-latitude continental margins, other sedimentological proxies are traditionally investigated to extract high-resolution records of ice and climate variability. Here we present a laser particle size record for the Early to Middle Miocene portion of the AND-2A core, drilled ~10 km from the East Antarctica coast (Harwood et al., 2009), and discuss its implications for the reconstruction of ice dynamics through the Miocene climatic optimum.

The AND-2A drill core was collected in 2007 by the Antarctic Geological Drilling Program (ANDRILL Southern McMurdo Sound Project) at 77°45.488′S, 165°16.605′E in Southern McMurdo Sound (SMS) in the western Ross Sea, which is connected to the Pacific Ocean (Fig. 1). Strata were recovered from the Victoria Land rift basin using a drill rig on a floating sea ice platform (~8.5 m thick) in ~383 m of water. The lithostratigraphy for the AND-2A core is characterized as cyclical successions of diamictites, conglomerates, sandstones, and mudrocks; diamictites were deposited primarily from floating ice (Fielding et al., 2008–2009; Passchier et al., 2011; Fig. 2A). The sediments are sourced from the Transantarctic Mountain

Figure 1. Location of the AND-2A drill site in Southern McMurdo Sound, Ross Embayment, Antarctica, and locations of nearby drill sites.
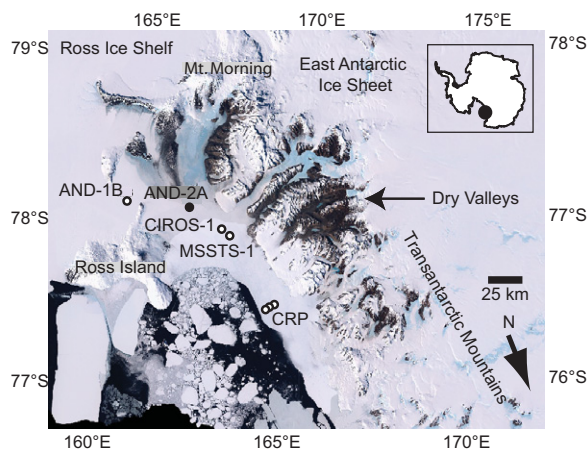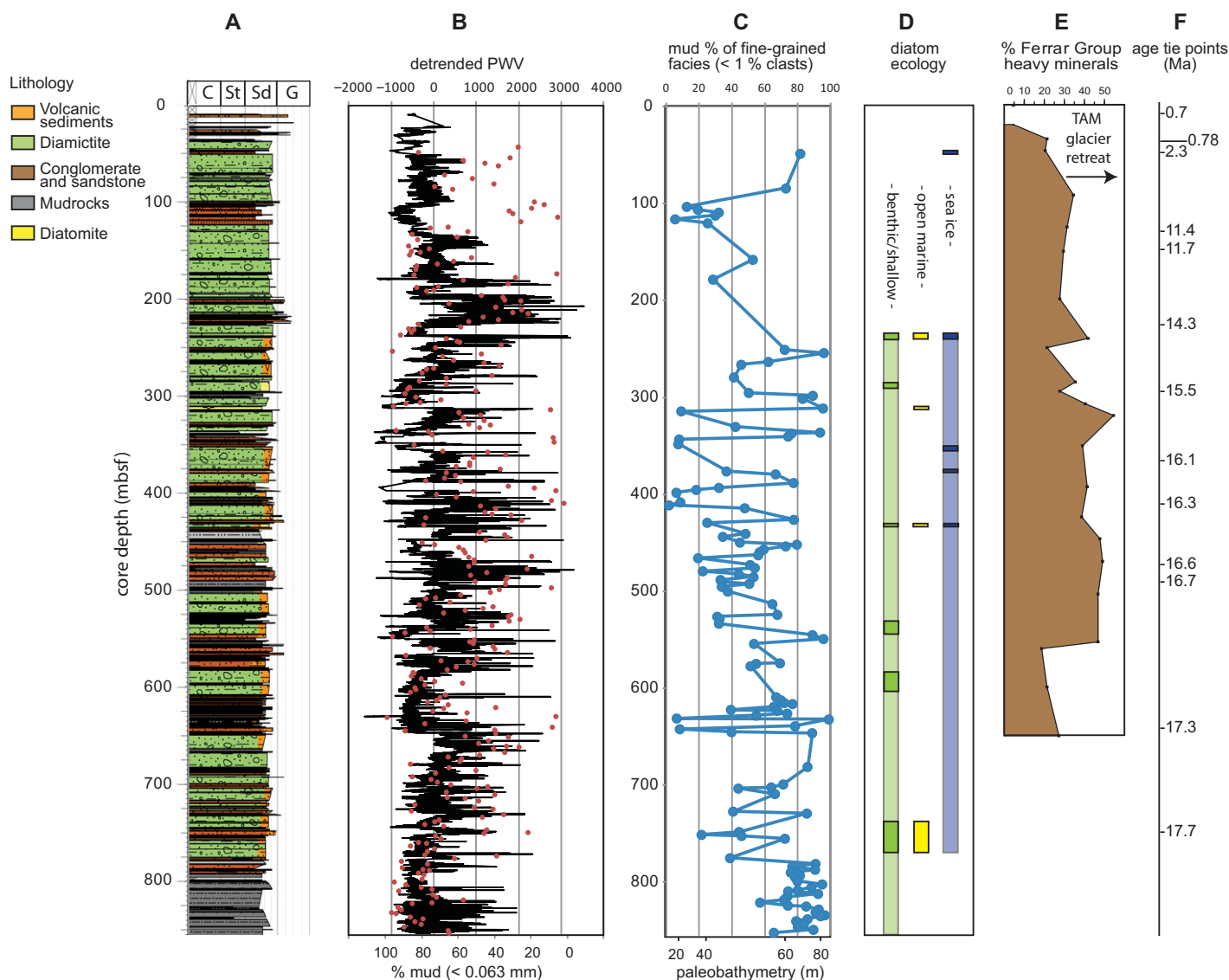
54

Figure 2. (A) Lithological column (Fielding et al., 2008–2009); mbsf—meters below seafloor; C—clay; St—silt; Sd—sand; G—gravel. (B) Downcore distribution of mud% (<0.063 mm) in <2 mm fraction plotted as red dots on top of detrended P-wave velocity (PWV; Dunbar et al., 2008–2009). (C) Average calculated apparent paleobathymetry. (D) Diatom ecology (Taviani et al., 2008–2009). (E) Percent heavy minerals of Ferrar Group provenance (Hauptvogel and Passchier, 2012). TAM—Transantarctic Mountains. (F) Age tie points (see Table 1). Apparent paleobathymetry (column C) is calculated for sandstones and mudstones with <1% clasts only and as an average for 2 wave climate scenarios (Manuwatu Coast, New Zealand, and Monterey Bay, California). Values deeper than 60 m represent minimum water depths (cf. Dunbar and Barrett, 2005). In the diatom ecology column, bars with solid colors represent samples with relatively well-preserved assemblages, whereas light colored bars represent intervals with samples having poorly preserved assemblages (data from Taviani et al., 2008–2009). There is generally a good correlation between lithology (A), mud%, and PWV (both in B), except in diatom-rich beds where the low specific density of biogenic silica distorts the correlation, and in isolated sections of disturbed core.

rift flank (Fielding et al., 2008; Miller et al., 2010), a mountain range with summit elevations higher than 4000 m.

METHODS

The AND-2A core was sampled at ~1 m intervals for particle size analysis in 2007, immediately after drilling, in McMurdo Station. The samples were split between three lab groups for particle size analysis, and we received samples at irregular 2–3 m spacing. More than 300 samples were processed by wet mechanical and chemical disaggregation (Konert and Vandenberghe, 1997). Previous studies using dry and wet disaggregation through crushing between wooden blocks, soaking in water with chemicals, and sonication yielded incomplete disaggregation for clay-rich samples (Fielding et al., 2001). We improved the sample disaggregation by replacing the initial dry crushing step by wet disaggregation with a mortar and pestle (De Groot, 2004). With this technique it is important to apply only gentle vertical motion to the sample with the pestle to avoid breaking grains. In the case that disaggregation was incomplete, samples were first soaked in water

for as long as several days before gentle wet dis-aggregation via mortar and pestle was repeated. The sediments were treated to remove organic and inorganic carbon and carbonate with H_2O_2 and HCl, following the procedures recommended in Konert and Vandenberghe (1997).

The grain size distribution of the gravel-free fraction (<2 mm) was determined using a dual light source Malvern Instruments Master-sizer 2000 laser particle size analyzer in the Sedimentology Laboratory at Montclair State University (Montclair, New Jersey), capable of measuring sediments with broad size ranges. The analyzer measures the entire particle size range from 0.02 to 2000 µm in one measurement. The dual light source set-up and improved software, including Mie theory, for the calculation of fine fraction distributions also avoids spurious modes encountered with single lens and single light source instruments, such as the Mastersizer X (Fielding et al., 2001; Dunbar and Barrett, 2005). Instrument settings followed the recommendations of Sperazza et al. (2004). Quality control was performed through repeat analysis of a fine-grained industrial standard QAS3002 and a natural fine sand standard Sandy Hook Dune 4.

Two age models were previously proposed for AND-2A, based on diatom biostratigraphy, magnetostratigraphy, [40]Ar/[39]Ar dating, [87]Sr/[86]Sr isotopic dating, fission track dating, and through correlation of compositional and physical properties of regional and global records (Acton et al., 2008–2009; Marcano et al., 2009; Di Vincenzo et al., 2010). One age model proposes a linear fit through the age tie points (Table 1) for the interval below 296 m below seafloor (mbsf), whereas an alternate age model incorporates a significant hiatus at 646 mbsf (Acton et al., 2008–2009; Di Vincenzo

et al., 2010). Spectral analysis of the particle size data between 646 and 296 mbsf was carried out for the two proposed age models using the REDFIT algorithms (Hammer et al., 2001; Schulz and Mudelsee, 2002), with varying overlapping segments and with a variety of smoothing windows (rectangular, Welch, triangle, and Hanning). The REDFIT algorithms overcome the problem of paleoclimate time series that are unevenly spaced in time by fitting a first-order autoregressive (AR1) process directly to the paleoclimate time series without the need of interpolation in the time domain. The program can be used to test if peaks in the spectrum of a time series are significant against the red-noise background from an AR1 process (Schulz and Mudelsee, 2002).

RESULTS

A total of 294 samples in the upper 855 m of the AND-2A core yielded particle size distributions for fully disaggregated sediments. Below 855.12 mbsf, pyrite cementation inhibited complete disaggregation. The sediments display large fluctuations in mud percent (mud%) (Fig. 2B) that correlate strongly to lithology (Fig. 2A), and for the interval below ~130 mbsf to the detrended P-wave velocity record (Fig. 2B) derived from multisensor track measurements on whole round cores (Dunbar et al., 2008–2009). Poor disaggregation of clay-rich samples has been observed in previous studies (Fielding et al., 2001), but our record does not display the expected spurious low mud percentages, where fine-grained lithologies are indicated (e.g., cf. high mud% below ~800 mbsf in Fig. 2B to gray mudstone in Fig. 2A). We conclude that our preparation procedure worked sufficiently well to disaggregate mud-rich samples. Downcore

variations of mud% in ice-distal facies (sandstones and mudstones with <1% clasts) show a general trend toward lower mud% between ~855 and 426 mbsf, with a minimum between ~585 and 311 mbsf (Fig. 2C). However, high-amplitude fluctuations are observed at ~650 mbsf and between ~426 and ~311 mbsf.

Spectral analysis of the mud% of the sediments in the well-dated interval 296–646 mbsf yielded similar results for the two age models (Acton et al., 2008–2009) and with different smoothing procedures. In the depth domain, cyclicity is found in the 16.7 m band using 3 overlapping segments and a Welch window (Fig. 3A). However, we suspect that the average 2.7 m (16 k.y.) sample spacing in the 296–646 mbsf interval inhibits recognition of shorter cycles; high power is also present in the 6.4 m band, but it does not exceed the false alarm level. The results for the linear age model predict cyclicity in the 99 k.y. band (Fig. 3B), while shorter cycles (94 k.y.) were observed for the piece-wise age model with hiatus at 646 mbsf (Fig. 3C). These cycle lengths are near short-eccentricity frequencies. High power in the 36–38 k.y. band (obliquity) is also observed, but it does not exceed the false alarm level (Figs. 3B, 3C). While our average sample spacing exceeds the Nyquist frequency for the obliquity signal, it is not sufficient to detect precession.

We recognize that aliasing of short orbital cyclicities (e.g., precession) can be a problem with low-resolution sampling of geological records along evenly spaced time intervals (Pisias and Mix, 1988). Our sampling, however, was carried out along irregularly spaced depth intervals, and samples are unevenly spaced in the time domain. To assess aliasing of the precession signal we sampled the Laskar et al. (2004) solution for precession at our sample depths in the time domain and conducted a REDFIT spectral analysis using both the linear and piece-wise age models (Figs. 4A, 4B). The resulting aliased precession frequencies are 83 k.y. for the linear age model and 66 and 37 k.y. for the piece-wise age model. These frequencies are significantly different from the 99 k.y. and 94 k.y. frequencies we find for the mud% data set. We conclude that aliasing of the precession signal is an unlikely contributor to the mud% cyclicity and that the signal can be attributed to variability in the short eccentricity band width.

SEDIMENTOLOGICAL INTERPRETATION OF THE PARTICLE SIZE DISTRIBUTIONS

Despite the glacial origin of the sediments in AND-2A, there is no correlation between sand percent and clast abundance or between sand and

TABLE 1. AGE TIE POINTS FOR AND-2A

Age young (Ma)	Age old (Ma)	Age used (Ma)	Depth of top (m)	Depth of bottom (m)	Depth used (m)	Description of datum*
0.640	0.740	0.691	10.22	10.24	10.23	[40]Ar-[39]Ar date on a lava clast
0.781	0.781	0.781	25.34	36.86	31.10	Chron C1N(o)
2.060	2.550	2.305	47.00	47.00	47.00	diatom assemblage
11.390	11.390	11.390	128.00	128.00	128.00	two [40]Ar-[39]Ar dates
10.550	12.950	11.670	144.03	144.06	144.05	Sr isotope date
14.290	14.290	14.290	225.38	225.38	225.38	LO *Denticulopsis maccollumii*
15.500	15.500	15.500	296.34	296.34	296.34	Diatom assemblage
15.750	16.400	16.050	366.80	366.85	366.83	Sr isotope date
16.268	16.268	16.268	412.00	414.52	413.26	C5Cn.1n(o)–C5Cn.1r(y)
16.543	16.543	16.543	446.95	451.37	449.16	C5Cn.2r(o)–C5Cr.3n(y)
16.721	16.721	16.721	486.68	489.74	488.21	C5Cn.3n(o) –C5Cr(y)
16.990	17.610	17.300	640.13	640.16	640.15	[40]Ar-[39]Ar date on tephra
17.717	17.717	17.717	748.25	750.55	749.40	C5Dr.1r(o)–C5Dr.1n(y)
17.740	17.740	17.740	757.08	761.42	759.25	C5Dr.1n(o)–C5Dr.2r(y)
19.660	20.360	20.010	1093.00	1093.04	1093.02	[40]Ar-[39]Ar date on tephra

Note: The AND-2A drill hole is part of the ANDRILL (Antarctic Geological Drilling Program) Southern McMurdo Sound Project. Depth of top designates the shallowest sample position for the datum and Depth of bottom the deepest position. The Depth used is the average depth used as a tie point for the datum in the age model.
*ChronC1N is Brunhes polarity chron (C—chronozones); LO—last occurrence. Data from Acton et al. (2008–2009), Marcano et al. (2009) and Di Vincenzo et al. (2010).
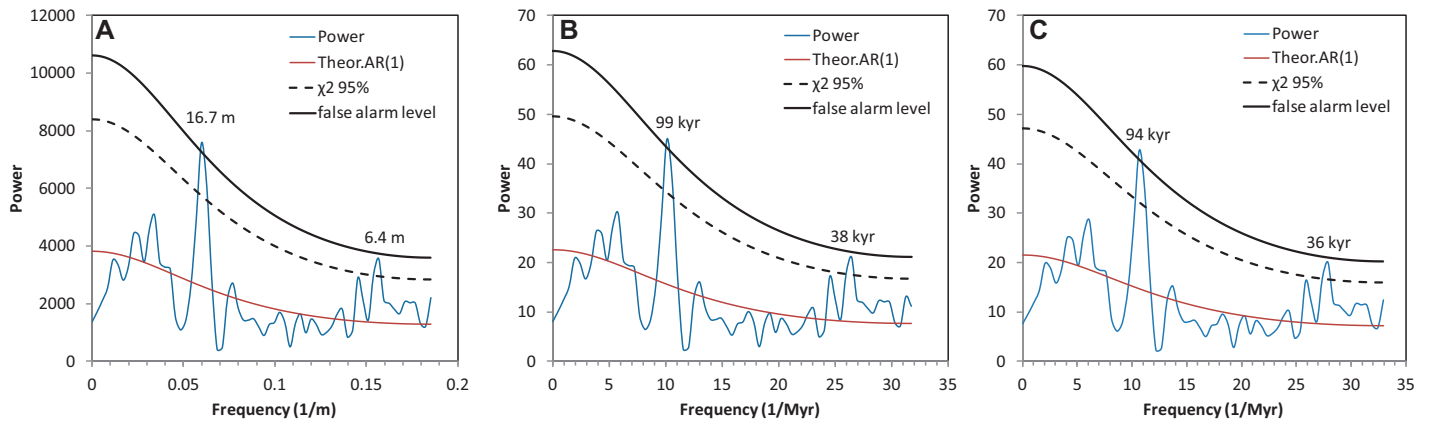
Figure 3. Spectral analysis of the mud% data series calculated from the laser particle size data for the well-dated interval 296–646 m below seafloor and using two different age models (Acton et al., 2008–2009). Smoothing with a Welch window and 3 segments provided significant results. Horizontal axes represent number of cycles per m or m.y. (A) In the depth domain, high power is observed in the 16.7 m band (τ = 2.0 m; false alarm = 98.5; see text). (B) In the time domain using the linear age model high power is observed in the 99 k.y. band, which is near characteristic lengths of short eccentricity (τ = 11.8 k.y.; false alarm = 98.5). (C) Using the piece-wise age model gave similar results with high power in the 94 k.y. band (τ = 11.3 k.y.; false alarm = 98.5). Theor.AR(1) represents a model of the climatic red-noise signature from a first-order autoregressive AR(1) process (Schulz and Mudelsee, 2002). τ designates the characteristic depth or time scale. The false-alarm level marks the maximum spectral amplitude that can be attributed to red noise in the data as predicted by the AR(1) model. $\chi2$ 95% indicates the 95% confidence limit for the autogressive process.

Figure 4. Aliasing frequencies of the precession signal for our sample spacing in the interval 296–646 m below seafloor, determined through spectral analysis of the Laskar et al. (2004) precession signal sampled at the particle size data points for the two different age models (Acton et al., 2008–2009). Horizontal axes represent number of cycles per m.y. (A) Using the linear age model significant power predicts aliasing in the 83 k.y. band (τ = 4.6 k.y.; false alarm = 98.5;

see text). (B) Using the piece-wise age model significant power predicts aliasing in the 66 and 37 k.y. bands (τ = 11.3 k.y.; false alarm = 98.5). Theor.AR(1) represents a model of the climatic red-noise signature from a first-order autoregressive AR(1) process (Schulz and Mudelsee, 2002). τ designates the characteristic time scale. The false-alarm level marks the maximum spectral amplitude that can be attributed to red noise in the data as predicted by the AR(1) model. $\chi2$ 95% indicates the 95% confidence limit for the autogressive process.
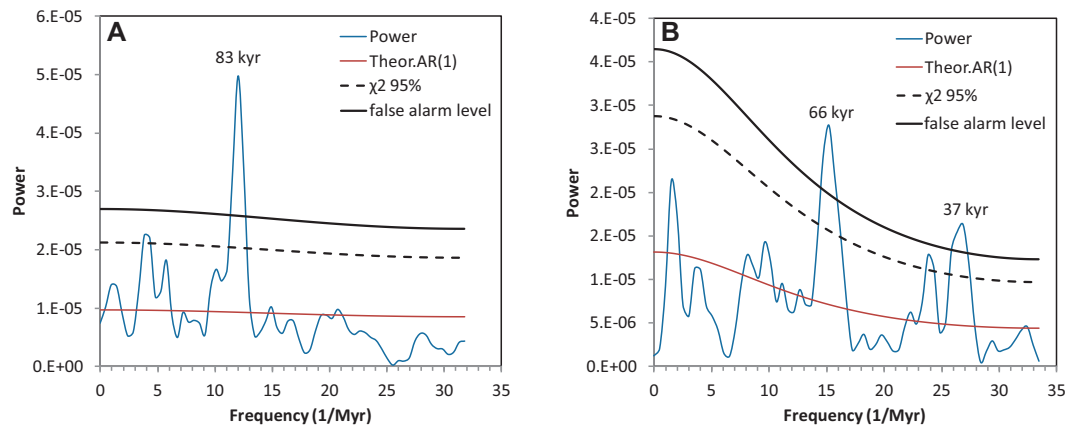
silt percent, in contrast to most glacially sourced hemipelagic sediments deposited in deep-marine environments (Hass, 2002). Particle sizes of the dominant lithology, diamictite, show a wide spread of sand percentages (<10% to >80%; Fig. 5), similar to those of Late Oligocene to Early Miocene massive diamicts of the nearby CIROS-1 and MSSTS-1 drill holes (Barrett, 1989). Principle component analysis reveals that nearly half (49%) of the variance in the particle size data set is controlled by the presence of a fine silt mode, and the absence of a fine to medium sand mode, suggestive of win-

nowing and bedload transport by waves or currents, respectively.

A total of 133 samples were taken from core sections with recognizable bedforms (cf. Passchier et al., 2011). Although some of the bedforms may have originated under an ice shelf, evidence of ice contact deposition is only interpreted at short intervals in the studied section, in the upper ~240 mbsf and locally between ~648 and 786 mbsf. The sedimentary section of the AND-2A core studied here (from 10 to 855 mbsf) consists of sediments deposited by polythermal or cold-based ice with significant

meltwater influence only below 800 mbsf (cf. Passchier et al., 2011). Most diamictites are stratified, and paleontological evidence suggests generally shallow, open-marine conditions, although the presence of fragments of diatoms with sea ice affinities indicates possible intermittent annual sea ice conditions between ~225 and 771 mbsf (Taviani et al., 2008–2009).

Within this framework, most of the planar and hummocky cross-stratification observed in sand-rich beds (Passchier et al., 2011) can be attributed to sheet flow induced by surface waves (Passchier and Kleinhans, 2005, and ref-
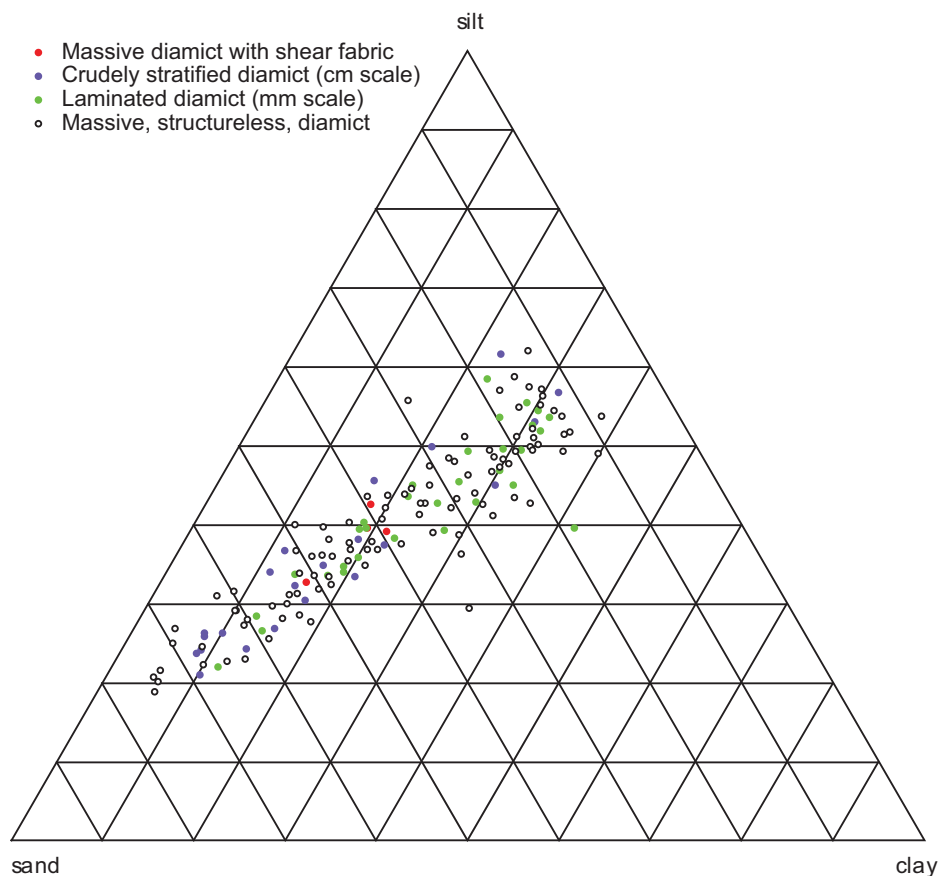
Figure 5. Ternary plot of sand-silt-clay percent of diamicts. Massive diamicts with shear fabrics are primary glacial tills. Laminated diamicts are generally more mud rich than primary tills, and most diamicts with crude stratification are more sand rich than primary tills and reflect the predominant influence of glaciomarine processes.

erences therein). Ripple cross-lamination and inclined bedding is typical of wave-, tide- and wind-driven current activity below wave base in coastal environments with a large sediment supply. In glacial coastal environments, ripples can originate from hyperpycnal flows generated by meltwater efflux. These bedforms, whether glacial or nonglacial in origin, are not sustainable under sheet flow and combined flow conditions near the wave base (Passchier and Kleinhans, 2005, and references therein). Crude planar stratification, which is typically found in diamictites in AND-2A, may indicate winnowing by waves or by wind- and tide-driven inner shelf currents. In contrast, the lamination in muddy diamictites and mudstones is more likely the result of suspension settling in cold or deep neritic shelf environments, where the influence of currents is diminished due to greater water depths or floating ice absorbing wave energy (Passchier et al., 2011).

The interpretation of the bedforms implies that the downcore variations in mud% in the AND-2A core primarily record changes in the intensity of wave stirring on a wave-dominated coast. Similar conclusions were previously reached for Oligocene and Early Miocene sediments in nearby drill holes (Barrett, 1989; De Santis and Barrett, 1998; Dunbar et al., 2008). The intensity of wave stirring is controlled on the one hand by changes in the wave climate determined by surface wind strength, sea ice coverage, and iceberg density, and on the other hand by paleobathymetry. It is unlikely that the full amplitude of changes in mud% (6%–96%) can be attributed to any of these effects alone. However, these processes are all linked to ice dynamics through the ice sheets effect on the high-latitude climate system.

WAVE CLIMATE

The geographic setting for southern McMurdo Sound in the Miocene was different from today, as the younger volcanic islands (visible in Fig. 1) did not yet exist (Di Vincenzo et al., 2010). Based on the paleotopographic evidence and the sedimentary facies in the AND-2A core, we

envision a relatively sediment-starved straight coastline along a wave-graded inner shelf with a moderate- to high-intensity wave climate. Paleoclimate modeling suggests that during the warmer than present Miocene climatic optimum, mid-latitude austral summer storm tracks were displaced poleward (Herold et al., 2011). However, in the Southern Hemisphere the intensity of the storms was diminished, according to the model, and the net effects on the wind fields around coastal East Antarctica translate into only small increases in wind speeds during the Miocene climatic optimum relative to today. The main control on the pressure gradients that drive the wind fields is the size of the ice sheet, and the wave stirring through a more intensive wind-driven wave climate increases in intensity as the ice sheet decreases in size.

Sea ice and floating glacial ice absorb wave energy and influence wave climate. Evidence for floating glacial ice comes from the gravel component of the diamictite-dominated succession of the AND-2A site (Passchier et al., 2011); episodic intensification of sea ice coverage is indicated by the presence of sea ice diatoms (Taviani et al., 2008–2009). A modeling study suggests that the formation of sea ice requires ice to be grounded in the Ross Sea (DeConto et al., 2007), a condition that would coincide with the production of floating glacial ice. Iceberg and sea ice production and survival is greatest for a large marine-based ice sheet. Therefore, the influence of floating ice on wave stirring is also controlled by the size of the ice sheet.

In summary, wave climate is controlled by the size of the ice sheet. A larger ice sheet decreases wave energy and wave stirring, resulting in high mud% in marine sediments, whereas a smaller ice sheet increases wave stirring, because of an increase in the pressure gradients and wind strength, coincident with a decrease in the effects of floating ice.

PALEOBATHYMETRY

Empirical relations between water depth and mud% with seaward fining have been found for low-latitude coasts under a variety of wave climates and are predicted by linear wave theory (Dunbar and Barrett, 2005; Ferré et al., 2005; Dunbar et al., 2008). The long-term trends in the intensity of wave stirring may be controlled by bathymetric changes related to tectonic or volcanic processes. Seismic data, however, suggest that the Victoria Land Basin was characterized by relatively constant and slow passive thermal subsidence in the late Early and Middle Miocene, with renewed rifting commencing later, ca. 13 Ma (Fielding et al., 2008). Extensive surface uplift and increased denudation of the

Transantarctic Mountains took place prior to the Miocene (Miller et al., 2010). Sediment accumulation rates were relatively constant and were not a major control on the paleobathymetry (Acton et al., 2008–2009). The expanded Miocene interval at the AND-2A site coincides with volcanic activity at the Mount Morning volcanic center, directly south of the drill site (Fig. 1), from ca. 19 Ma (Di Vincenzo et al., 2010) with possible crustal loading or flexure.

On time scales shorter than 1 m.y., the paleobathymetry of the AND-2A site was potentially affected by ice dynamics as a consequence of the exponential increase in the self-gravitation effect in the direction of the center of an ice mass, which at this latitude could be larger than the eustatic signal (Gomez et al., 2010). Through geodynamic modeling, Gomez et al. (2010) demonstrated that ice mass loss in the Wilkes subglacial basin area of East Antarctica would result in sea-level fall in the vicinity of the AND-2A drill site due to the combined effects of eustasy, glacioisostasy, and self-gravitation. The imprint of the evolution of local sea level near the margin of a continental-scale ice sheet on glaciomarine sedimentation was hypothesized by Boulton (1990). First, upon glacial advance,

the migration of a peripheral forebulge several hundreds of kilometers ahead of the advancing ice margin causes a minor temporary fall of relative sea level (Fig. 6, early glacial stage). Despite uncertainties in the lithospheric properties of this margin, the effects of forebulge migration at the location of the AND-2A drill site are likely to be small due to its ice-proximal inner shelf position with respect to the largest ice mass. Second, in response to ice growth, advance, and grounding on the shelf, a deepening of the glacially influenced area is predicted as a result of glacioisostatic crustal depression and self-gravitation (Fig. 6, early glacial stage). In the proglacial marine zone, proximal to the maximum ice extent, local sea-level rise precedes the glacial maximum, resulting in deposition of thick units of glaciomarine diamicts (Fig. 6, glacial maximum stage). Upon glacial retreat, rapid crustal rebound, initially to several meters per year (Fig. 6, late glacial stage), with rates declining as the ice mass decreases, results in rapid shoaling of the depositional environment with sand- and gravel-rich coastal facies deposited as a regressive sequence (Fig. 6, postglacial stage). The lithostratigraphy of the AND-2A site is dominated by glaciomarine diamict, mud, and

stratified coastal sandstones (Passchier et al., 2011), in agreement with the sedimentation model presented by Boulton (1990).

CALCULATED APPARENT PALEOBATHYMETRY FOR ICE-DISTAL FACIES

The wave climate for ice-distal facies with <1% gravel clasts was less likely affected by floating ice absorbing wave energy. The increase in wind strength for the Miocene climatic optimum is quite small (Herold et al., 2011). Although we recognize the uncertainties introduced by these variables, we believe that it is possible to estimate the paleobathymetry for the ice-distal facies (Fig. 2C) using empirical relations between water depth and mud% derived from modern low-latitude coasts (Dunbar and Barrett, 2005). Attributing all changes in mud% to variable wave stirring controlled by water depth, we calculated paleobathymetry and analyzed its downcore pattern for ice-distal facies only (Fig. 2C). As suggested in Dunbar et al. (2008), we calculated the average paleobathymetry using equations based on low-latitude circum-Pacific coasts with moderate and
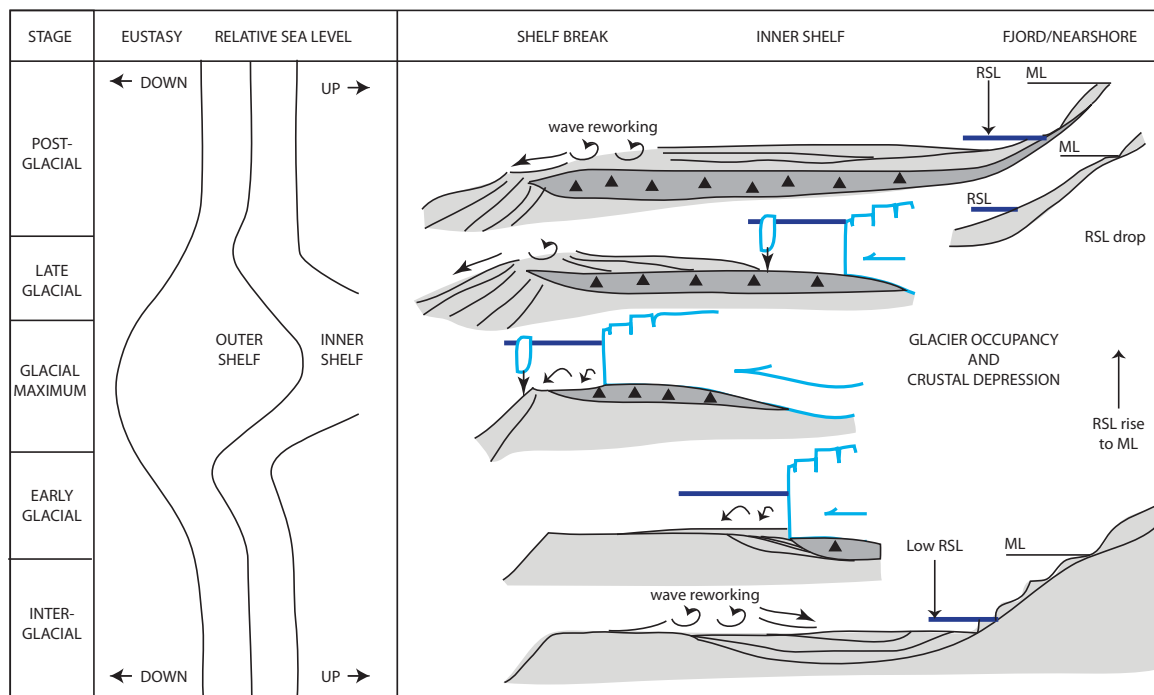

Figure 6. Sedimentation model in response to ice growth and decay and associated relative sea-level variations near the center of a large continental ice sheet (modified after Boulton, 1990). From bottom to top, the figure illustrates ice extent and relative sea level (RSL) changes through a glacial cycle. The left panel illustrates the more or less opposite behavior of global (eustatic) versus high-latitude relative sea-level variations due to the combined effects of self-gravitation and glacioisostasy near the margin of an ice sheet. The right panel is a schematic model of the resulting paleobathymetric changes and sedimentation patterns through a glacial cycle. The dark blue line marks RSL within each stage of the glacial cycle. ML is marine limit, the maximum RSL reached during glacial advance.

high wave climates, i.e., Manuwatu coast in New Zealand and Monterey Bay in California.

Samples taken from intervals with bedforms generate calculated paleo–water depths from the particle size distributions that realistically position the bedforms in a sequence with respect to average fair weather (~25 m) and storm wave base (~40 m) on a shoreface to offshore transect (Fig. 7). The calculated water depths for the average of the two end-member wave scenarios applied to ice-distal facies in the AND-2A site range from 12 to 88 m (Fig. 2C). The implication is that the water depth in the Miocene in southern McMurdo Sound was at least ~300 m shallower than the current water depth of 383 m. Alternatively, Southern McMurdo Sound could have had a more extreme wave climate than envisioned by us and others (Barrett, 1989; Dunbar et al., 2008), much more severe than that of the Pacific Coasts today. However, even with a poleward displacement of mid-latitude storms during the warmer than present Miocene climatic optimum, waves capable of moving sediment at 300 m water depth are not realistic, given the modeled wind strength (Herold et al., 2011). Moreover, our interpretations are in agreement with evidence from ichnofossils and paleontology (Fielding et al., 2008–2009; Taviani et al., 2008–2009). The presence of shallow-water diatoms, such as *Palaia* sp., in many samples in the upper 775 m of the core (Taviani et al., 2008–2009) requires periodically shallow (<100 m depth) open-water conditions.

HIGH-AMPLITUDE CHANGES AND ORBITAL CYCLICITY IN MUD%

It is very unlikely that the short-lived and high-amplitude changes in mud% can be attributed to tectonic processes or associated paleotopographic or paleobathymetric changes affecting wave climate, but paleobathymetric changes associated with the geodynamic effects of ice growth and decay operate on shorter time scales. Fortunately, the paleobathymetric effects of geodynamic changes in inner shelf settings (Boulton, 1990; cf. Fig. 6) reinforce the effects of wave climate on the mud%; deepening during glacial phases produces mud-rich strata and shoaling during interglacial phases produces sand-rich strata, although the magnitude of change will depend on the position of the changing ice mass relative to the drill site. Therefore, despite uncertainties in the dominant control on the particle size changes, i.e., geodynamic effects on the paleobathymetry or wave climate influenced by floating ice or wind strength, we are confident that high-latitude ice volume changes are the ultimate forcing factor of the changes in mud%.

The interval with mud% minima (ice decay) between ~585 and 311 mbsf (ca. 17–15.7 Ma; Fig. 2C) in the AND-2A core anticorrelates to abundances of heavy minerals sourced from the Ferrar Group (Fig. 2E) that were interpreted as indicating ice sheet retreat into the upland regions of the Transantarctic Mountains (Hauptvogel and Passchier, 2012). We interpret that the high-amplitude changes in mud% in ice-distal facies (Fig. 2C) between 426 and 311 mbsf (ca. 16.3 and ca. 15.7 Ma) can be attributed to increased wave stirring (low mud%) reflecting a combination of shoaling of the inner shelf due to geodynamic effects of ice decay coincident with a slight increase in wave climate during interglacials, followed by decreased wave stirring (high mud%) reflecting the effects of deepening and intermittent sea ice formation during episodes of ice growth. It is interesting that the intensity of wave stirring minima reflected in the mud% of ice-distal facies decreases from the height of the Miocene climatic optimum ca. 16.3 Ma into the Middle Miocene (Fig. 2C).

The dominant lithofacies in the AND-2A core is diamictite (Passchier et al., 2011). However, the lack of a glacial signature in the particle size distributions and the presence of bedforms in diamictites suggest that currents and waves were significantly modifying grain size distributions for these facies as well. The complete record of mud% for all samples including diamictites reflects a pattern broadly similar to that of the ice-distal facies alone. Applying both age models (Acton et al., 2008–2009), episodes of low mud% coincide with eccentricity lows ca. 17.8 Ma and between 16.7 and 15.7 Ma (Fig. 8). Although we cannot quantify the relative contributions of changes in wave climate and paleobathymetry to the intensity of wave stirring reflected in the mud%, as discussed herein, both variables are ultimately forced by the size of the ice sheet. The cyclicity in the 99 or 94 k.y. band can therefore be interpreted as a reflection of high-latitude climate and ice volume, which are intimately linked.

PALEOCLIMATIC IMPLICATIONS

The orbitally paced changes in mud% in the AND-2A core represent the first near-field evidence for a dynamic ice sheet coinciding with the late Early Miocene climatic optimum (Flower and Kennett, 1994). The interpretations of the mud% in the AND-2A core reflecting wave stirring of decreasing intensity at ice sheet minima between ca. 16.3 and 15.7 Ma are in agreement with regional and global records of ice growth and decay. From ca. 17 Ma onward the Antarctic ice sheet retreated from the continental shelf into the upland regions of the Transantarctic Mountains,
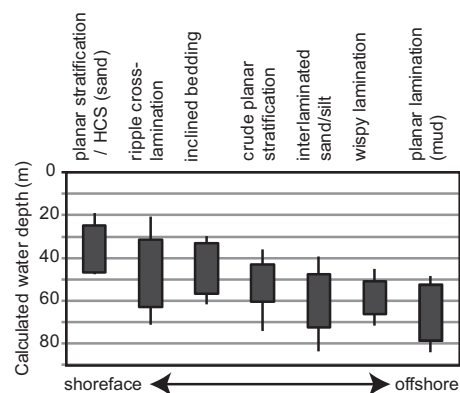

Figure 7. Calculated water depths for the 133 samples taken from core with recognizable bedforms. HCS—hummocky cross-stratification.

and the process of considerable thickening of the East Antarctic ice sheet for it to overtop some of the mountains and to become grounded on the shelf in the Ross Sea did not begin until after ca. 15 Ma (Lewis et al., 2007; Passchier et al., 2011; Hauptvogel and Passchier, 2012). The data are also in partial agreement with combined back-stripping and oxygen isotope records of the Australian Marion Plateau and other low-latitude continental margins (Kominz et al., 2008; John et al., 2011) that document a 54–69 m eustatic change between 16.5 and 13.9 Ma over 4 separate events reflecting a stepwise and increasing amplitude of ice growth, separated by episodes of eustatic rise indicating ice decay. However, as discussed herein, geodynamic modeling suggests that eustasy is not likely a major driver of wave energy in our record (Gomez et al., 2010), and the link between the records is an ice volume signal expressed differently at low- and high-latitude margins.

In the late Early Miocene, the thermal isolation of Antarctica was well on its way; most tectonic and sedimentary evidence indicates opening and deep flow through the Drake Passage since ca. 23–16 Ma (Barker et al., 2007; Lyle et al., 2007) and a transition to polythermal glaciers with some freezing in the marginal areas by ca. 18 Ma (Passchier et al., 2011). It is interesting that in the Southern Ocean, Early and Middle Miocene decreases in $\delta^{18}O_{seawater}$, interpreted as episodic ice decay, coincided with surface- and bottom-water cooling events (Shevenell et al., 2008), which Holbourn et al. (2005) attributed to melting pulses of the Antarctic ice sheet under severe summer melt as orbital eccentricity increased (Fig. 8). The facies in the AND-2A core, however, do not provide evidence of higher surface melt rates in the late Early and Middle Miocene (Passchier
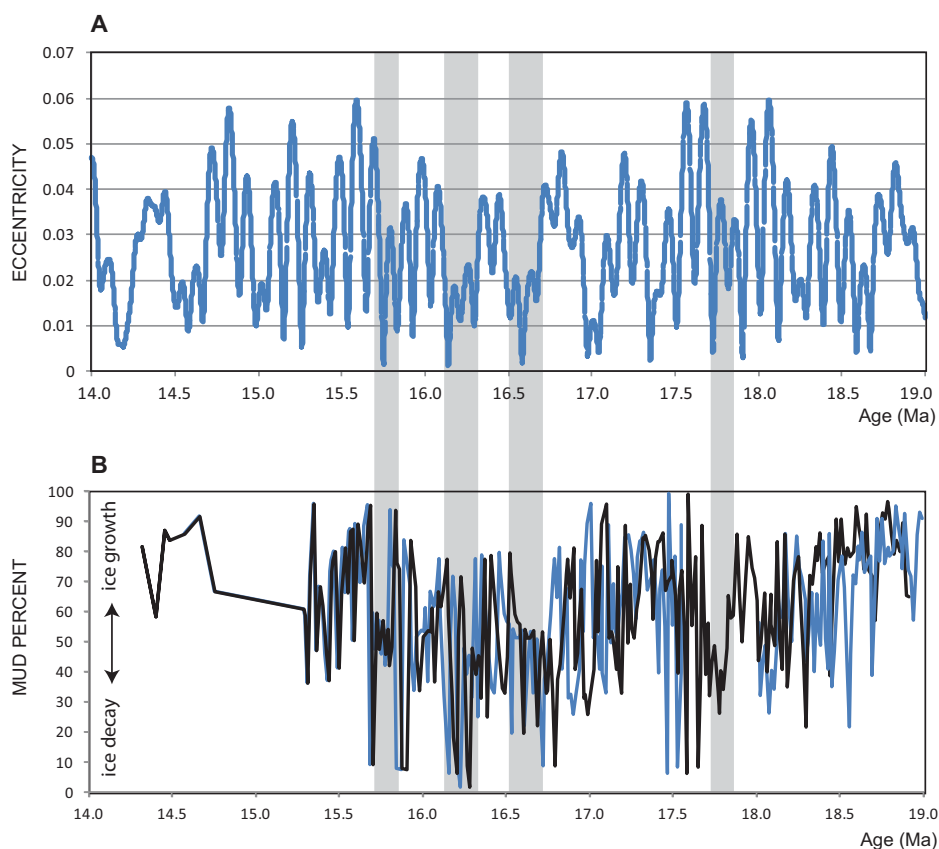
A

B

Figure 8. (A) Eccentricity as calculated from Laskar et al. (2004). (B) Mud percent of samples in the AND-2A core plotted versus age on the linear age model (black) and the piecewise age model (blue) (Acton et al., 2008–2009). Vertical gray bars indicate a correlation between eccentricity lows and low mud% (ice decay) in AND-2A.

CONCLUSIONS

We discuss a laser particle size record of the AND-2A core on the Antarctic continental shelf and its implications for Miocene ice development from a high-latitude site. Abrupt shifts in mud% within glacial-interglacial cycles mark the record between ca. 16.7 and 15.7 Ma. We attribute these to the combined effects of episodic changes in ice coverage of surface waters, storm activity, and paleobathymetry associated with ice sheet instability in Antarctica during the Miocene climatic optimum. Changes in mud% are orbitally paced with significant power in the short-eccentricity band. In addition, ice sheet minima coincide with eccentricity minima indicative of far-field forcing. In the absence of strong evidence for extensive late Early and Middle Miocene surface melt in the lithofacies of the AND-2A core (Passchier et al., 2011), we attribute the cycles of ice growth and decay to fluctuations in marine ice sheet instability in response to changes in ocean circulation and heat transport.

REFERENCES CITED

Acton, G., Florindo, F., Jovane, L., Lum, B., Ohneiser, C., Sagnotti, L., Strada, E., Verosub, K.L., Wilson, G.S., and the ANDRILL-SMS Science Team, 2008–2009, Preliminary integrated chronostratigraphy of the AND-2A Core, ANDRILL Southern McMurdo Sound Project, Antarctica, *in* Harwood, D.M., et al., eds., Studies from the ANDRILL Southern McMurdo Sound Project, Antarctica—Initial Science Report on AND-2A: Terra Antartica, v. 15, p. 211–220, doi:2122/6034.

Barker, P.F., Filippelli, G.M., Florindo, F., Martin, E.E., and Scher, H.D., 2007, Onset and role of the Antarctic Circumpolar Current: Deep-Sea Research Part II, v. 54, p. 2388–2398, doi:10.1016/j.dsr2.2007.07.028.

Barrett, P.J., 1989, Sediment texture, *in* Barrett, P.J., ed., Antarctic Cenozoic history from the CIROS-1 drillhole, McMurdo Sound: DSIR Bulletin, v. 245, p. 49–58.

Billups, K., and Shrag, D., 2002, Paleotemperatures and ice volume of the past 27 Myr revisited with paired Mg/Ca and ^{18}O/^{16}O measurements on benthic foraminifera: Paleoceanography, v. 17, 1003, doi:10.1029/2000PA000567.

Boulton, G.S., 1990, Sedimentary and sea level changes during glacial cycles and their control on glacimarine facies architecture, *in* Dowdeswell, J.A., and Scourse, J.D., eds., Glaciomarine environments: Processes and sediments: Geological Society of London Special Publication 53, p. 15–52, doi:10.1144/GSL.SP.1990.053.01.02.

et al., 2011), and we show that pronounced ice retreat–induced wave stirring is observed during short-eccentricity minima between ca. 16.7 and 15.7 Ma (Fig. 8).

During eccentricity minima the seasonality in the Southern Hemisphere is diminished, with relatively cool summers promoting a positive surface mass balance for the Antarctic ice sheet. To explain the depleted oxygen isotope values in late Early Miocene deep-sea cores of the Southern Ocean, some have proposed a role for injection of relatively warm waters, such as the Tethyan Indian Saline Water, at intermediate depth into the Antarctic circumpolar circulation (Woodruff and Savin, 1989; Flower and Kennett, 1994; Shevenell et al., 2008). Another important factor for the Miocene scenario may have been the opening of Fram Strait in the North Atlantic ca. 17.5 Ma (Jakobssen et al., 2007) that significantly enhanced the oceanic meridional heat transport. The entrainment of corrosive North Atlantic bottom waters within the Antarctic circumpolar circulation is supported by the presence of eccentricity-paced deep-ocean carbonate

dissolution events in the Miocene record of the southeastern Pacific (Ocean Drilling Program Site 1237; Holbourn et al., 2007). Driven by the southward migration of atmospheric frontal systems during the Miocene climatic optimum (Herold et al., 2011), incursions of relatively warm Circumpolar Deep Water onto the overdeepened Antarctic shelf may have been capable of destabilizing marine-grounded ice margins in West Antarctica (Jacobs et al., 2011) or in the Wilkes and Aurora subglacial basins (Gomez et al., 2010; Young et al., 2011). Today, the presence of a thermocline between fresh, cold, Antarctic surface waters and relatively warm, salty, Circumpolar Deep Water 600–700 m beneath the surface near marine-grounded ice allows for a scenario of sub–ice shelf melt without significant surface melt (Jacobs et al., 2011). We therefore conclude that a possible explanation for the Antarctic ice retreat phases during eccentricity minima of the Miocene climatic optimum is a Northern Hemisphere forcing of the temperature of the Circumpolar Deep Water and its effect on marine-grounded ice margins.

DeConto, R., Pollard, D., and Harwood, D., 2007, Sea ice feedback and Cenozoic evolution of Antarctic climate and ice sheets: Paleoceanography, v. 22, PA3214, doi:10.1029/2006PA001350.

De Groot, P.A., 2004, Handbook of stable isotope analytical techniques, Volume 1: Amsterdam, Elsevier, 1258 p.

De Santis, L., and Barrett, P.J., 1998, Grain size analysis of samples from CRP-1: Terra Antartica, v. 5, p. 375–382.

Di Vincenzo, G., Bracciali, L., Del Carlo, P., Panter, K., and Rocchi, S., 2010, ^{40}Ar/^{39}Ar laser dating of volcanogenic products from the AND-2A core (ANDRILL Southern McMurdo Sound Project, Antarctica): Bulletin of Volcanology, v. 72, p. 487–505, doi:10.1007/s00445-009-0337-z.

Dunbar, G.B., and Barrett, P.J., 2005, Estimating paleobathymetry of wave-graded continental shelves from sediment texture: Sedimentology, v. 52, p. 253–269, doi:10.1111/j.1365-3091.2004.00695.x.

Dunbar, G.B., Naish, T.R., Barrett, P.J., Fielding, C.R., and Powell, R.D., 2008, Constraining the amplitude of late Oligocene bathymetric changes in Western Ross Sea during orbitally-induced oscillations in the East Antarctic Ice Sheet: (1) Implications for glacimarine sequence stratigraphic models: Palaeogeography, Palaeoclimatology, Palaeoecology, v. 260, p. 50–65, doi:10.1016/j.palaeo.2007.08.018.

Dunbar, G., Atkins, C., Magens, D., Niessen, F., and the ANDRILL-SMS Science Team, 2008–2009, Physical properties of the AND-2A core, ANDRILL Southern McMurdo Sound Project, Antarctica, *in* Harwood, D.M., et al., eds., Studies from the ANDRILL Southern McMurdo Sound Project, Antarctica—Initial Science Report on AND-2A: Terra Antartica, v. 15, p. 49–56.

Ferré, B., Guizien, K., Durrieu de Madron, X., Palanques, A., Guillén, J., and Grémare, A., 2005, Fine-grained sediment dynamics during a strong storm event in the inner shelf of the Gulf of Lion (NW Mediterranean): Continental Shelf Research, v. 25, p. 2410–2427, doi:10.1016/j.csr.2005.08.017.

Fielding, C.R., Dunbar, G.B., and Bryce, S.M., 2001, Laser-derived particle size data from CRP-3, Victoria Land Basin, Antarctica: Implications for sequence and seismic stratigraphy: Terra Antartica, v. 8, p. 255–262.

Fielding, C.R., Whittaker, J., Henrys, S.A., Wilson, T.J., and Naish, T.R., 2008, Seismic facies and stratigraphy of the Cenozoic succession in McMurdo Sound, Antarctica: Implications for tectonic, climatic and glacial history: Palaeogeography, Palaeoclimatology, Palaeoecology, v. 260, p. 8–29, doi:10.1016/j.palaeo.2007.08.016.

Fielding, C.R., 10 others, and the ANDRILL-SMS Science Team, 2008–2009, Sedimentology and stratigraphy of the AND-2A core, ANDRILL Southern McMurdo Sound, Project, Antarctica, *in* Harwood, D.M., et al., eds., Studies from the ANDRILL Southern McMurdo Sound Project, Antarctica—Initial Science Report on AND-2A: Terra Antartica, v. 15, p. 77–112.

Flower, B.P., and Kennett, J.P., 1994, The middle Miocene climatic transition: East Antarctic ice sheet development, deep ocean circulation and global carbon cycling: Palaeogeography, Palaeoclimatology, Palaeoecology, v. 108, p. 537–555, doi:10.1016/0031-0182(94)90251-8.

Foster, G.L., Lear, C., and Rae, J.W., 2012, The evolution of pCO$_2$, ice volume and climate during the middle Miocene: Earth and Planetary Science Letters, v. 341–344, p. 243–254, doi:10.1016/j.epsl.2012.06.007.

Gomez, N., Mitrovica, J.X., Tamisiea, M.E., and Clark, P.U., 2010, A new projection of sea-level change in response to collapse of marine sectors of the Antarctic Ice Sheet: Geophysical Journal International, v. 180, p. 623–634, doi:10.1111/j.1365-246X.2009.04419.x.

Hammer, Ø., Harper, D.A.T., and Ryan, P.D., 2001, PAST: Paleontological Statistics Software Package for education and data analysis: Palaeontologia Electronica, v. 4, 9 p., http://palaeo-electronica.org/2001_1/past/issue1_01.htm.

Harwood, D., Florindo, F., Talarico, F., Levy, R., Kuhn, G., Naish, T., Niessen, F., Powell, R., Pyne, A., and Wilson, G., 2009, Antarctic drilling recovers stratigraphic records from the continental margin: Eos (Transactions, American Geophysical Union), v. 90, p. 90, doi:10.1029/2009EO110002.

Hass, C., 2002, A method to reduce the influence of ice-rafted debris on a grain-size record from northern Fram Strait, Arctic Ocean: Polar Research, v. 21, p. 299–306, doi:10.1111/j.1751-8369.2002.tb00084.x.

Hauptvogel, D.W., and Passchier, S., 2012, Early–Middle Miocene (17–14 Ma) Antarctic ice dynamics reconstructed from the heavy mineral provenance in the AND-2A drill core, Ross Sea, Antarctica: Global and Planetary Change, v. 82–83, p. 38–50, doi:10.1016/j.gloplacha.2011.11.003.

Herold, N., Huber, M., and Mueller, R.D., 2011, Modeling the Miocene climatic optimum, Part 1: Land and atmosphere: Journal of Climate, v. 24, p. 6353–6372, doi:10.1175/2011JCLI4035.1.

Holbourn, A., Kuhnt, W., Schulz, M., and Erlenkeuser, H., 2005, Impacts of orbital forcing and atmospheric carbon dioxide on Miocene ice-sheet expansion: Nature, v. 438, p. 483–487, doi:10.1038/nature04123.

Holbourn, A., Kuhnt, W., Schulz, M., Flores, J.-A., and Andersen, N., 2007, Orbitally-paced climate evolution during the middle Miocene "Monterey" carbon-isotope excursion: Earth and Planetary Science Letters, v. 261, p. 534–550, doi:10.1016/j.epsl.2007.07.026.

Jacobs, S., Jenkins, A., Giulvi, C.F., and Dutrieux, P., 2011, Stronger ocean circulation and increased melting under Pine Island Glacier ice shelf: Nature Geoscience, v. 4, p. 519–523, doi:10.1038/ngeo1188.

Jakobsson, M., Backman, J., Rudels, B., Nycander, J., Frank, M., Mayer, L., Jokat, W., Sangiorgi, F., O'Regan, M., Brinkhuis, H., King, J., and Moran, K., 2007, The Early Miocene onset of a ventilated circulation regime in the Arctic Ocean: Nature, v. 447, p. 986–990, doi:10.1038/nature05924.

John, C.M., Karner, G.D., Browning, E., Leckie, R.M., Mateo, Z., Carson, B., and Lowery, C., 2011, Timing and magnitude of Miocene eustasy derived from the mixed siliciclastic-carbonate stratigraphic record of the northeastern Australian margin: Earth and Planetary Science Letters, v. 304, p. 455–467, doi:10.1016/j.epsl.2011.02.013.

Kominz, M.A., Browning, J.V., Miller, K.G., Sugarman, P.J., Mizintseva, S., and Scotese, C.R., 2008, Late Cretaceous to Miocene sea-level estimates from the New Jersey and Delaware coastal plain coreholes: An error analysis: Basin Research, v. 20, p. 211–226, doi:10.1111/j.1365-2117.2008.00354.x.

Konert, M., and Vandenberghe, J., 1997, Comparison of laser grain size analysis with pipette and sieve analysis; a solution for the underestimation of the clay fraction: Sedimentology, v. 44, p. 523–535, doi:10.1046/j.1365-3091.1997.d01-38.x.

Laskar, J., Robutel, P., Joutel, F., Gastineau, M., Correia, A.C.M., and Levrard, B., 2004, A long term numerical solution for the insolation quantities of the Earth: Astronomy & Astrophysics, v. 428, p. 261–285, doi:10.1051/0004-6361:20041335.

Lewis, A.R., Marchant, D.R., Ashworth, A.C., Hemming, S.R., and Machlus, M.L., 2007, Major middle Miocene global climate change: Evidence from East Antarctica and the Transantarctic Mountains: Geological Society of America Bulletin, v. 119, p. 1449–1461, doi:10.1130/0016-7606(2007)119[1449:MMMGCC]2.0.CO;2.

Lyle, M., Gibbs, S., Moore, T.C., Jr., and Rea, D.K., 2007, Late Oligocene initiation of the Antarctic Circumpolar Current: Evidence from the South Pacific: Geology, v. 35, p. 691–694, doi:10.1130/G23806A.1.

Marcano, M.C., Mukasa, S., Lohmann, K.C., Stefano, C., Taviani, M., and Andronikov, A., 2009, Chronostratigraphic and paleoenvironmental constraints derived from the ^{87}Sr/^{86}Sr and δ^{18}O signal of Miocene bivalves, Southern McMurdo Sound, Antarctica: Global and Planetary Change, v. 69, p. 124–132, doi:10.1016/j.gloplacha.2009.05.001.

Miller, S.R., Fitzgerald, P.G., and Baldwin, S.L., 2010, Cenozoic range-front faulting and development of the Transantarctic Mountains near Cape Surprise, Antarctica: Thermochronologic and geomorphologic constraints: Tectonics, v. 29, TC1003, doi:10.1029/2009TC002457.

Naish, T.R., and 32 others, 2001, Orbitally induced oscillations in the East Antarctic Ice Sheet at the Oligocene/Miocene boundary: Nature, v. 413, p. 719–723, doi:10.1038/35099534.

Passchier, S., and Kleinhans, M.G., 2005, Observations of sand waves, megaripples and hummocks in the Dutch coastal area and their relation to currents and combined flow conditions: Journal of Geophysical Research, v. 110, F04S15, doi:10.1029/2004JF000215.

Passchier, S., Browne, G., Field, B., Fielding, C.R., Krissek, L.A., Panter, K., Pekar, S.F., and ANDRILL-SMS Science Team, 2011, Early and middle Miocene Antarctic glacial history from the sedimentary facies distribution in the AND-2A drill hole, Ross Sea, Antarctica: Geological Society of America Bulletin, v. 123, p. 2352–2365, doi:10.1130/B30334.1.

Pisias, N.G., and Mix, A.C., 1988, Aliasing of the geologic record and the search for long-period Milankovitch cycles: Paleoceanography, v. 3, p. 613–619, doi:10.1029/PA003i005p00613.

Schulz, M., and Mudelsee, M., 2002, REDFIT: Estimating red-noise spectra directly from unevenly spaced paleoclimatic time series: Computers & Geosciences, v. 28, p. 421–426, doi:10.1016/S0098-3004(01)00044-9.

Shevenell, A.E., Kennett, J.P., and Lea, D.W., 2008, Middle Miocene ice sheet dynamics, deep-sea temperatures, and carbon cycling: A Southern Ocean perspective: Geochemistry Geophysics Geosystems, v. 9, p. 1–14, doi:10.1029/2007GC001736.

Sperazza, M., Moore, J.N., and Hendrix, M.S., 2004, High-resolution particle size analysis of naturally occurring very fine-grained sediment through laser diffractometry: Journal of Sedimentary Research, v. 74, p. 736–743, doi:10.1306/031104740736.

Taviani, M., 18 others, and the ANDRILL-SMS Science Team, 2008–2009, Palaeontological characterisation and analysis of the AND-2A core, ANDRILL Southern McMurdo Sound Project, Antarctica, *in* Harwood, D.M., et al., eds., Studies from the ANDRILL Southern McMurdo Sound Project, Antarctica—Initial Science Report on AND-2A: Terra Antartica, v. 15, p. 113–146.

Woodruff, F., and Savin, S., 1989, Miocene deepwater oceanography: Paleoceanography, v. 4, p. 87–140, doi:10.1029/PA004i001p00087.

Young, D.A., Wright, A.P., Roberts, J.L., Warner, R.C., Young, N.W., Greenbaum, J.S., Schroeder, D.M., Holt, J.W., Sugden, D.E., Blankenship, D.D., van Ommen, T.D., and Siegert, M.J., 2011, A dynamic early East Antarctic Ice Sheet suggested by ice-covered fjord landscapes: Nature, v. 474, p. 72–75, doi:10.1038/nature10114.